Astron. Astrophys. 318, 579–594 (1997)

ASTRONOMY
AND
ASTROPHYSICS

# Chemical inhomogeneities in interstellar clouds: the high latitude cloud MCLD 123.5+24.9

**M. Gerin[1,2], E. Falgarone[2], K. Joulain[2], M. Kopp[3], J. Le Bourlot[3], G. Pineau des Forêts[3], E. Roueff[3], and P. Schilke[4]**

[1] Downs Laboratory of Physics, Caltech, Physics Department, 320-47, Pasadena, CA 91125, USA
[2] Radioastronomie Millimétrique, Laboratoire de Physique de l'ENS, 24 rue Lhomond, F-75231 Paris Cedex 05, France. URA336 du CNRS
[3] DAEC, Observatoire de Paris-Meudon, Place J. Janssen, F-92195 Meudon cedex, France. URA 0173 du CNRS
[4] I. Physikalisches Institut der Universität zu Köln, Zülpicher Str. 77, D-50937 Köln, Germany.

Received 26 February 1996 / Accepted 21 May 1996

**Abstract.** We report on observations designed to disclose the presence of the High Ionization Phase predicted to exist in dark clouds by chemical models (Le Bourlot et al. 1993). In addition to a high neutral carbon abundance, a high CS/SO abundance ratio and a low abundance of molecular ions, such a phase might be characterized by a low D/H fractionation ratio.
In this paper, we present both observational and model results on the sulfur bearing molecules CS and SO, and their most abundant isotopomers, on the molecular ions $HCO^+$, $H^{13}CO^+$, $HC^{18}O^+$ and $DCO^+$. We have also taken new $^{13}CO$ and $C^{18}O$ data to improve the determination of the physical conditions at the observed positions. One of the two dark clouds investigated, a core in the high latitude cloud MCLD 123.5+24.9, presents surprinsingly strong CS and $^{34}CS$ lines relative to its column density, together with weak $DCO^+$ lines. It has also a cold temperature and rather strong CCH and $C_3H_2$ lines. These observed features are characteristic of the presence of the High Ionization Phase along the line of sight. This cloud core might therefore be a good candidate for further investigation of this new phase of dark interstellar clouds.

**Key words:** molecular processes – ISM: MCLD 123.5+24.9; abundances; clouds; molecules – radio lines: molecules

## 1. Introduction

As the angular resolution of the millimetric observations of molecular clouds has increased, a common finding has been the ubiquitous existence of small scale structure in maps of molecular emission lines, down to the angular resolution. In such maps, the structure, when clearly self-similar, is thought to arise primarily from the action of turbulence, coupled to small-scale abundance variations related to chemical processes and excitation effects related to the structure of the cloud itself (density, temperature, velocity field, overall size). However, because the presence of molecules allows the gas to cool more efficiently, abundance and excitation effects are linked and act together to produce the observed line maps. Indeed, it is now obvious that maps of different molecular tracers coincide grossly at large scale ($\geq 1$ pc) but exhibit conspicuous differences at small scale ($\leq 0.5$ pc). These differences cannot be explained by radiative transfer only since maps of optically thin transitions also differ (Ungerechts et al. 1995). It is also difficult to assign them to fluctuations of the illuminating UV radiation field because of their small scale. The most obvious explanation is therefore the presence of abundance variations in dark clouds, which do not seem related to the overall physical conditions of the clouds. Indeed, true chemical differences have been found in e.g. TMC1 and L134N (Olano et al. 1988; Hirahara et al. 1992; Swade 1989a,b). These abundance variations may be linked to different elemental abundances in different clouds, as investigated by e.g. Langer & Graedel (1989). Time dependent chemistry has also been invoked as an explanation for both the chemical differences between clouds and the high abundance of hydrocarbons (Herbst & Leung 1989; Millar et al. 1987). Some other mechanisms have recently been proposed to generate chemical heterogeneities inside dark clouds. The role of turbulent transport has been investigated by Chièze et al. (1991) as a source of reactive species (C, $C^+$) deep inside the clouds where these species no longer exist at steady state because the ionization flux is too low. In this perspective, the past history of gas fragments may be important to determine the current molecular abundances. Diffusion of reactive species due to turbulence is expected to alter significantly the steady state solutions of dark cloud chemistry and to predict a larger neutral carbon abundance throughout dark clouds (Xie et al. 1995). Abundance gradients as a function of extinction are then expected to be smoothed by the turbulent diffusion process.

However, the existence of abundance variations might be deeply rooted in the chemical network itself, as shown by the discovery of chemical bistability for the range of physical parameters of dark molecular clouds (Pineau des Forêts et al. 1992;

*Send offprint requests to*: M. Gerin, French address

Le Bourlot et al. 1993b; Flower et al. 1994; Le Bourlot et al. 1995a,b). Because chemical reactions are highly non linear, and can be seen from a mathematical point of view as a dissipative process, a non regular behaviour is to be expected for certain values of the model parameters, which include the physical parameters of the cloud but also all the reaction rates. The most remarkable issue is then that the bifurcation between two stable solutions occurs in the range of densities and cosmic rays ionization rate $\zeta$ typical of dark interstellar clouds (Le Bourlot et al. 1995a). In this range, two stable phases are predicted to coexist. These phases differ mostly by their ionization fraction which in turn affects a large number of molecular abundances. The Low Ionization Phase (LIP) is the already known solution of gas-phase chemical models characterized by a low ionization ($[e^-] \leq 10^{-7}$). Its chemistry is driven by ion-molecule reactions among which proton transfer reactions due to $H_3^+$ play a major role. The gas phase neutral carbon abundance is low because all available gas phase carbon (either C or $C^+$) ends up in forming the very stable carbon monoxyde CO, by means of reactions of C and $C^+$ with $O_2$ and $H_2O$ which are abundant in this phase. One major problem with this steady state solution is that it predicts far too low abundances of complex hydrocarbons in e.g. TMC1 (Hirahara et al. 1992). Moreover, all the observations of neutral carbon in dark molecular clouds reveal large neutral carbon abundances which cannot be easily reproduced by the above classical models (Phillips & Huggins 1981; Keene 1995; Schilke et al. 1995).

On the contrary, $H^+$ is the dominant ion in the High Ionization Phase (HIP) and the electronic abundance reaches $10^{-6}$. In that case, water vapor and molecular oxygen are mostly destroyed by reactions with $H^+$ and $C^+$, and no longer formed. $H_3^+$ is destroyed by recombination with electrons. This phase is thus characterized by a high C/CO abundance ratio in the gas phase and thus a slightly lower gas temperature due to the presence of carbon which acts as an additional coolant. The molecular species most affected by the switch in the chemistry are the molecular ions such as $H_3^+$, $HCO^+$ and $N_2H^+$, the sulfur bearing molecules CS and SO, and hydrocarbons such as CCH. CS is formed through reactions involving C and $C^+$ and its abundance may be increased in the HIP. SO, which is formed through neutral-neutral reactions with OH and other oxygenated molecules, is efficiently destroyed by atomic and ionic carbon and its abundance is largely decreased in the HIP. The presence of energy barriers on the route to SO and its formation via OH explains the sensitivity of this species to the steady-state solution.

There is no straightforward way to test observationally the existence of bistability in dark clouds due to the expected mixture of the two phases on any line of sight and the interplay discussed above between the chemistry and other physical processes in the clouds. We have used the result presented in Fig. 6a of Le Bourlot et al. (1995) which states that the higher the CR ionization rate $\zeta$, the higher the expected fraction of HIP in a cloud, all other control parameters being the same, to increase the probability to intercept a HIP fragment on the line of sight. We have selected two dark cloud cores with presumably different cosmic rays ionization rates $\zeta$, to be able to compare with the LIP. The first one, in the high latitude cloud MCLD 123.5+24.9, close to the North Galactic Pole and the Polaris star, lies within a prominent high latitude HI loop associated with a supernova remnant (Heiles 1976). For this field (called Polaris throughout the paper), the value of $\zeta$ is probably higher than the average value in the local interstellar medium.

**Table 1.** Source parameters

| | Polaris | Taurus |
|---|---|---|
| Coordinates | $l_{II}$ = 123.68 | RA(1950) = 04 34 07 |
| | $b_{II}$ = 24.930 | DEC(1950) = 24 10 00 |
| $V_{LSR}$ (km s$^{-1}$) | −4.5 | 6.0 |
| Reference position (arcsec) | (1200,−680) | (0,−500) |
| Distance (pc) | 100 | 150 |

The other field lies in the Taurus complex and may have an average value of $\zeta$ since this complex has no clear connexion with any supernova remnant. We refer to this second field as Taurus. Both fields lie at comparable distances. The coordinates are reported in Table 1, together with the LSR velocities, offsets for reference positions and cloud distances. For these two targets, we have observed the same set of CS and SO lines, $HCO^+$ and the simplest carbon chain CCH. The observations are described in Sect. 2 and the results are given in Sect. 3. In Sect. 4, we present a comparison of these two fields with other dark clouds, and discuss in Sect. 5 possible observational tests of bistability.

## 2. Observations

We observed at the IRAM 30 m telescope at Pico Veleta (Spain) during two observing runs in March 1994 and July 1995. The receivers were SIS mixers with SSB noise temperatures of about 100 K to 150 K at 3 mm, 2 mm and 1.3 mm. The system temperatures were 280, 270 and 600 K at 3 mm, 2 mm and 1.3 mm respectively for the March 1994 observations. All spectra were taken in position switching mode, with the reference positions given in Table 1. In July 1995, we observed at 3 mm and 2 mm only. The system temperatures were 200 K at 3 mm and 250 K at 2 mm. We used frequency switching or position switching to subtract the atmospheric emission. The frequency throw was set to a few MHz, usually 7.3 MHz. As a backend, we used a digital correlator with frequency resolution of 20 kHz or 40 kHz and total number of channel 1024 per frequency analysed. This enabled us to observe simultaneously lines close enough in frequency to fit in the 512 MHz instantaneous bandwidth of the receivers: the $^{13}$CO(1–0) and C$^{18}$O (1–0) lines and the C$^{18}$O(2–1) and SO($6_5$-$5_4$) lines were observed this way. We checked the pointing on nearby continuum sources and planets. The pointing was stable with typical pointing errors of less than 3″ for the July 1995 run and less than 5″ for the March 1994 run.

Because the clouds are much more extended than the telescope beam, we present all results in the $T_A^*$ scale. For those readers which prefer to use the main beam temperature scale, the 30 m main beam efficiencies are 0.70, 0.55 and 0.40 at

**Table 2.** Observed molecular lines. Adopted dipole moments: $\mu$(CS) = 2.0 Debye, $\mu$(SO) = 1.55 Debye, $\mu(HCO^+)$ = 3.9 Debye, $\mu(DCO^+)$ = 3.7 Debye, $\mu$(CCH) = 0.8 Debye, $\mu(C_3H_2)$ = 3.3 Debye, $\mu(HCS^+)$ = 1.9 Debye

| Species | Transition | Frequency (GHz) | $E_u$ (K) | A ($s^{-1}$) |
|---|---|---|---|---|
| $^{12}C^{32}S$ | 2–1 | 97.980968 | 7.05 | $1.68\ 10^{-5}$ |
| $^{12}C^{32}S$ | 3–2 | 146.969049 | 14.1 | $6.07\ 10^{-5}$ |
| $^{12}C^{32}S$ | 5–4 | 244.935606 | 23.5 | $2.98\ 10^{-4}$ |
| $^{12}C^{34}S$ | 2–1 | 96.412982 | 6.94 | $1.60\ 10^{-5}$ |
| $^{12}C^{34}S$ | 3–2 | 144.617147 | 13.9 | $5.79\ 10^{-5}$ |
| $^{13}C^{32}S$ | 2–1 | 92.494299 | 6.66 | $1.41\ 10^{-5}$ |
| $^{32}SO$ | $3_2$–$2_1$ | 99.299879 | 9.23 | $1.15\ 10^{-5}$ |
| $^{32}SO$ | $4_3$–$3_2$ | 138.178648 | 15.9 | $3.23\ 10^{-5}$ |
| $^{32}SO$ | $6_5$–$5_4$ | 219.949391 | 35.0 | $1.36\ 10^{-4}$ |
| $^{34}SO$ | $3_2$–$2_1$ | 97.715388 | 9.23 | $1.09\ 10^{-5}$ |
| $^{34}SO$ | $4_3$–$3_2$ | 135.775633 | 15.9 | $3.07\ 10^{-5}$ |
| $HCO^+$ | 1–0 | 89.188523 | 4.28 | $4.19\ 10^{-5}$ |
| $H^{13}CO^+$ | 1–0 | 86.754330 | 4.16 | $3.86\ 10^{-5}$ |
| $HC^{18}O^+$ | 1–0 | 86.162157 | 4.13 | $3.76\ 10^{-5}$ |
| $DCO^+$ | 2–1 | 144.077321 | 10.4 | $1.91\ 10^{-4}$ |
| CCH | 3/2,2–1/2,1 | 87.316925 | 4.19 | $4.12\ 10^{-7}$ |
| CCH | 3/2,1–1/2,0 | 87.328624 | 4.19 | $3.42\ 10^{-7}$ |
| $C_3H_2$ | $2_{1,2}$–$1_{0,1}$ | 85.33890 | 4.1 | $2.51\ 10^{-5}$ |
| $HCS^+$ | 2–1 | 85.34790 | 6.1 | $1.00\ 10^{-5}$ |

3 mm, 2 mm and 1.3 mm respectively. Given the difference in forward efficiencies, the antenna temperatures at 3 mm, 2 mm and 1.3 mm have to be multiplied by 1.3, 1.6 and 2.1 respectively to be converted to main beam brightness temperatures.

In each cloud, we observed a few positions to check for the presence of small scale variations of molecular line emission. In this paper, we present results for two positions in the Taurus field and three positions in the Polaris field, separated by about 40″.

## 3. Column densities and abundances

### *3.1. Spectroscopic parameters*

The spectroscopic parameters of the observed lines other than CO and isotopomers are gathered in Table 2. Because CS and SO have nearly the same weight and dipole moment, the energy level spacings and Einstein coefficients are roughly the same, thus we expect to observe lines of comparable intensities towards clouds where both molecules have similar abundances. However, because SO has a permanent spin the rotational levels are split and two quantum numbers (the total angular momentum and the rotational angular momentum) are necessary to describe the molecule. The SO spectrum is therefore richer than the CS spectrum and the opacity of each line may be lower than the opacity of the corresponding CS rotational line.

### *3.2. Data*

We have reduced the spectra of both observing runs by combining individual scans and removing linear or when possible zero order baselines. The spectra taken in frequency switching mode generally suffered from poorer base lines than the spectra in position switching mode. But we always tried to use a safe part of the band where the base line was flat. Figures 1, 2 show representative spectra for Taurus and Polaris respectively. Despite the similarity of the $^{13}$CO (1–0) and (2–1) profiles for both sources, the CS and CCH lines are strikingly different, with much stronger signals towards Polaris than towards Taurus.

To extract information from the spectra, we fitted a Gaussian profile on the reduced spectra. Except for some $^{12}$CO spectra which required at least two Gaussian components, all spectra were reasonably well fitted by one Gaussian profile. The results of the Gaussian fits are gathered in Tables 3 and 4 for the Taurus and Polaris fields respectively. Note that for Polaris, we have used some data from the IRAM Key Project (Falgarone et al. 1996).

### *3.3. Physical conditions and column densities*

To derive the physical conditions in the clouds and the abundances, we have used an LVG model with a kinetic temperature of 10 K. Such a low kinetic temperature is supported by the intensity of the $^{12}$CO lines and the environment of the clouds, with a low ambient radiation field. Moreover, previous observations of the high latitude cloud MCLD 123.5+24.9 provide constraints on the kinetic temperature $6\,K \leq T_K \leq 15\,K$ from CO and $NH_3$ data (Grossmann & Heithausen 1992). As for the Taurus field, 10 K is a typical value, used for many investigations of dark cloud cores in the Taurus complex. We have also estimated column densities under the assumption of LTE for some weak lines. The column densities derived from the observations are gathered in Table 5 for both clouds. Column densities derived from a similar LVG analysis at $T_K$=15 K are lower by 10–20% whereas the densities are lower by about 50%.

#### 3.3.1. $^{13}$CO and C$^{18}$O

For the Polaris field, the $^{13}$CO and C$^{18}$O data are fitted with an $H_2$ density ranging between 3 000 and 5 000 $cm^{-3}$ for $^{13}$CO and between 4 000 and 7 000 $cm^{-3}$ for C$^{18}$O. The weakness of the $^{13}$CO (3–2) lines detected by Heithausen et al. (1995) is consistent with such densities. In that case, the $^{13}$CO column densities are about $6\ 10^{15}$ $cm^{-2}$.

The C$^{18}$O column densities are about $8\ 10^{14}$ $cm^{-2}$. Thus the [$^{13}$CO]/[C$^{18}$O] abundance ratio is fairly uniform at a value of 7.5 for the three studied points. This value is slightly larger than the terrestrial double isotopic ratio $\frac{[^{13}C]}{[^{12}C]} \times \frac{[^{16}O]}{[^{18}O]} = 500/89 = 5.6$ but comparable to the expected abundance ratio (500/70 = 7.1) if the actual value of the [$^{12}$C]/[$^{13}$C] abundance ratio in the interstellar medium has decreased since the formation of the solar system and is now about 70 (Wilson and Rood 1994). This [$^{13}$CO]/[C$^{18}$O] abundance ratio indicates that $^{13}$CO and C$^{18}$O

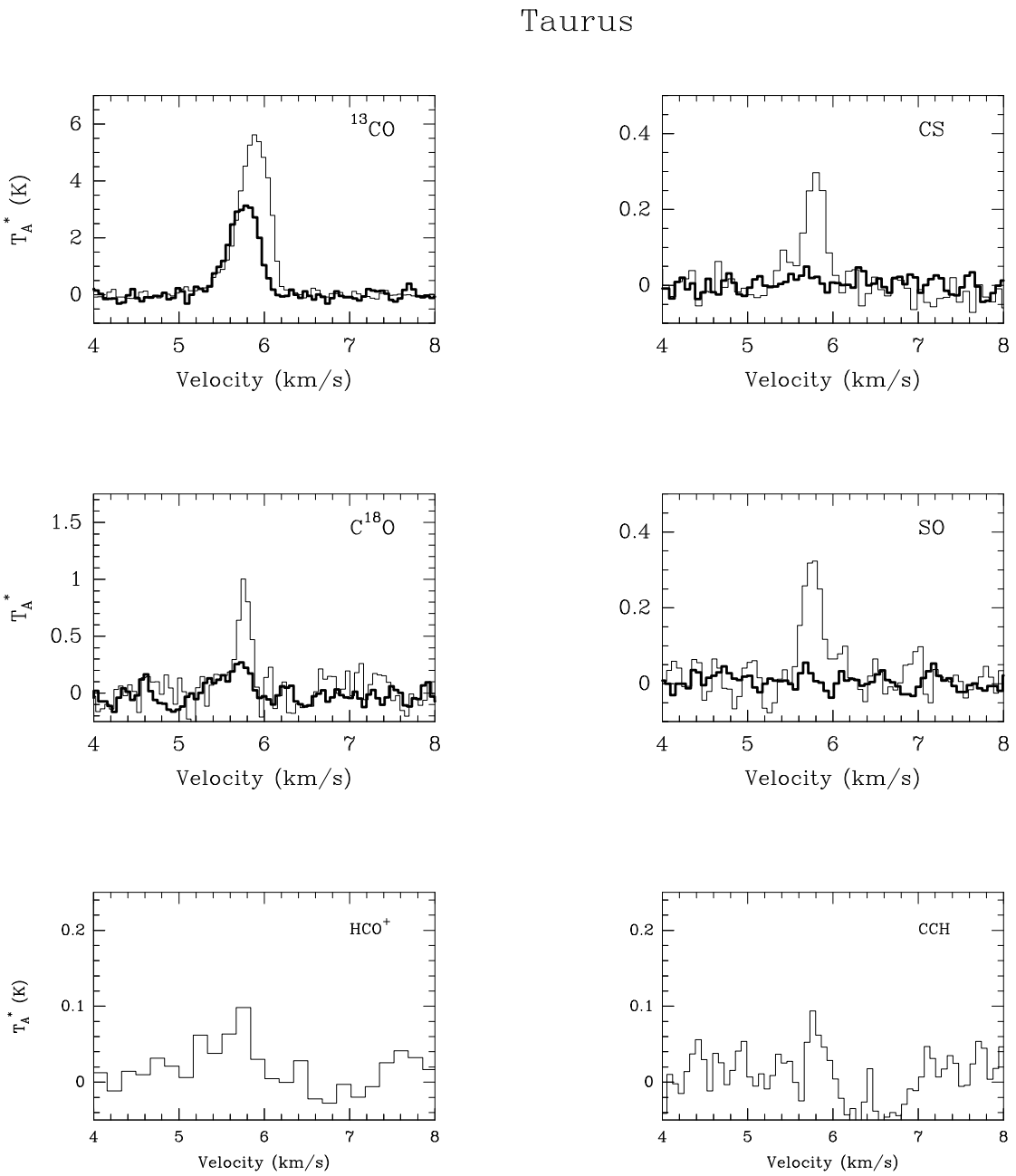


**Fig. 1.** Spectra towards the position (0″,-180″) in Taurus. All spectra are given in the $T_A^*$ temperature scale, the velocity scale is $V_{LSR}$. Top left: $^{13}$CO(1–0) thin line and (2–1) thick line, Middle left: C$^{18}$O(1–0) thin line and (2–1) thick line, Top right: CS(2–1) thin line and C$^{34}$S (2–1) thick line, Middle right: SO($3_2 - 2_1$) thin line and $^{34}$SO($3_2 - 2_1$) thick line. Bottom left: HCO$^+$(1–0), Bottom right: CCH(3/2–1/2)

have reached their dark cloud abundances and that no fractionation or selective photodissociation mechanisms are taking place. Thus the core of this high latitude cloud is similar to a dark cloud. Indeed, the C$^{18}$O abundance relative to $H_2$ deduced from the LVG model and with a velocity gradient of 2.3 km s$^{-1}$ pc$^{-1}$ (Heithausen et al. 1995), is between 2 and 3 $10^{-7}$, a value similar to dark cloud values, 1–3 $10^{-7}$ (Frerking et al. 1982; Duvert et al. 1986).

From the $^{13}$CO and C$^{18}$O data we can estimate the $H_2$ column density for the cloud core and the total extinction, using either relative abundances or the relationships between visible extinction and molecular line intensities and column densities. Using a $^{13}$CO relative abundance of 1.5 $10^{-6}$, we obtain N($H_2$) = 4 $10^{21}$ cm$^{-2}$ which corresponds to an extinction of 4 mag. Using the relationships between extinction and molecular column density found by Lada et al. (1994), Duvert et al. (1986), Cernicharo & Guélin (1987), and Frerking et al. (1982), the extinction toward the Polaris core is derived to be 3–5 mag from $^{13}$CO and 4–6 mag from C$^{18}$O. Thus we adopt a mean value of

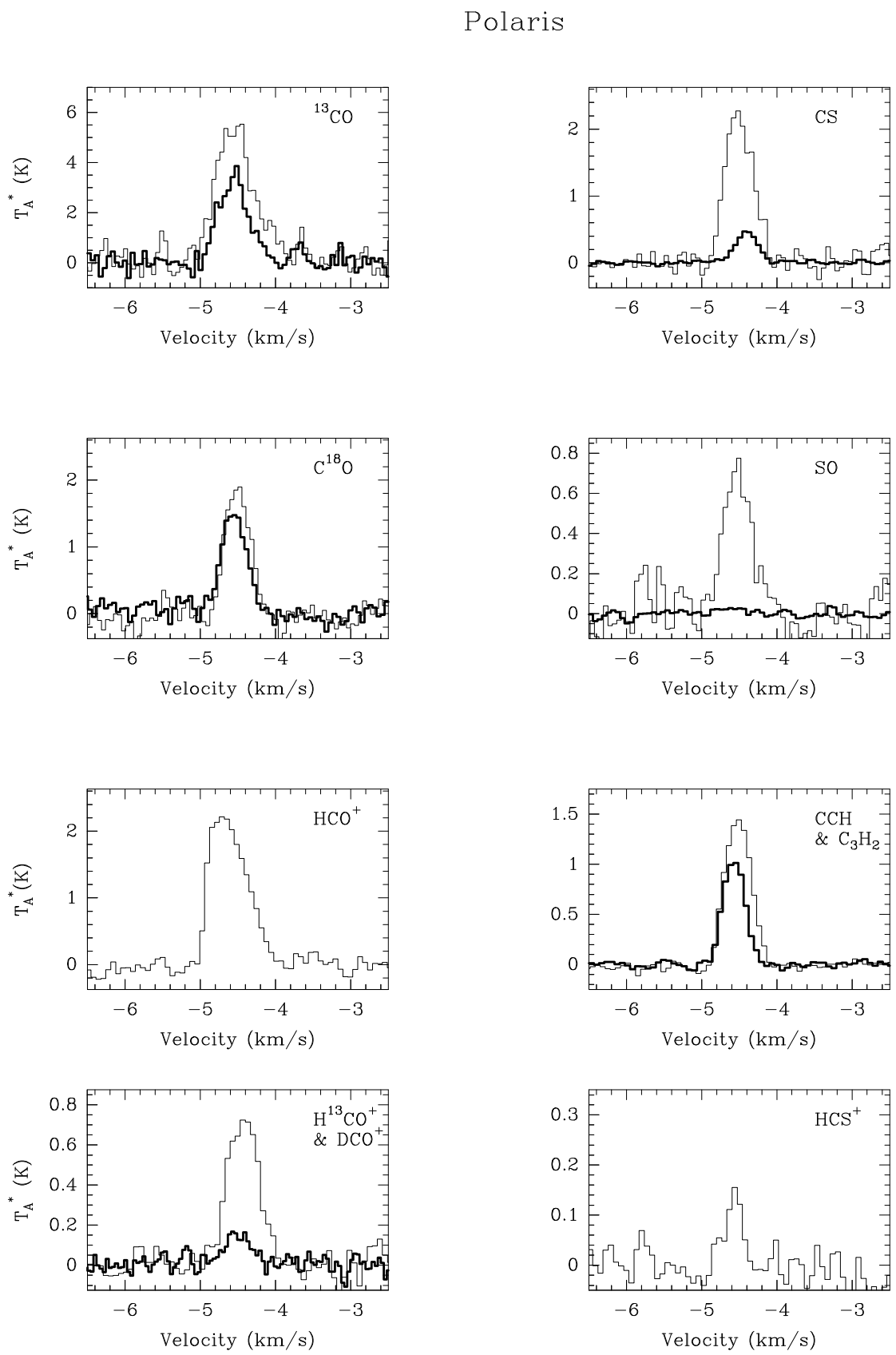


**Fig. 2.** Spectra towards the position (37.5″,7.5″) in Polaris. All spectra are given in the $T_A^*$ temperature scale, the velocity scale is $V_{LSR}$. Top left: $^{13}$CO(1–0) thin line and (2–1) thick line, Middle left: C$^{18}$O(1–0) thin line and (2–1) thick line, Top right: CS(2–1) thin line and C$^{34}$S (2–1) thick line, Middle right: SO($3_2 - 2_1$) thin line and $^{34}$SO($3_2 - 2_1$) thick line. Third row left: HCO$^+$(1–0), Bottom left: H$^{13}$CO$^+$(1–0) thin line and DCO$^+$(2–1) thick line, third row right: CCH(3/2–1/2) thin line and $C_3H_2$ ($2_{12} - 1_{01}$) thick line, Bottom right: HCS$^+$(2–1)

**Table 3.** Observed data towards Taurus

| Line | (0″,−180″) | | | | (0″,−190″) | | | |
|---|---|---|---|---|---|---|---|---|
| | $\int T_A^* dv$ (K km s$^{-1}$) | $T_{max}$ (K) | $\Delta v$ (km s$^{-1}$) | $\sigma$ (mK) | $\int T_A^* dv$ (K km s$^{-1}$) | $T_{max}$ (K) | $\Delta v$ (km s$^{-1}$) | $\sigma$ (mK) |
| $^{13}$CO(1–0) | 2.4 | 5.7 | 0.40 | 103 | | | | |
| $^{13}$CO(2–1) | 1.4 | 3.3 | 0.41 | 125 | 1.3 | 3.4 | 0.37 | 89 |
| C$^{18}$O(1–0) | 0.18 | 1.0 | 0.18 | 140 | | | | |
| C$^{18}$O(2–1)[a] | 0.08 | 0.23 | 0.34 | 42 | 0.08 | 0.23 | 0.34 | 42 |
| CS(2–1) | 0.09 | 0.30 | 0.27 | 35 | 0.08 | 0.33 | 0.24 | 61 |
| CS(3–2) | 0.034 | 0.11 | 0.3 | 14 | $\leq$ 0.06 | $\leq$ 0.21 | | 71 |
| CS(5–4) | $\leq$ 0.12 | $\leq$ 0.4 | | 130 | | | | |
| C$^{34}$S(2–1) | $\leq$ 0.018 | $\leq$ 0.06 | | 20 | | | | |
| C$^{34}$S(3–2) | $\leq$ 0.021 | $\leq$ 0.07 | | 23 | | | | |
| SO($3_2$–$2_1$) | 0.10 | 0.33 | 0.27 | 51 | 0.08 | 0.35 | 0.22 | 55 |
| SO($4_3$–$3_2$) | 0.02 | 0.17 | 0.11 | 30 | 0.016 | 0.17 | 0.09 | 48 |
| $^{34}$SO($3_2$–$2_1$) | $\leq$ 0.018 | $\leq$ 0.06 | | 20 | | | | |
| $^{34}$SO($4_3$–$3_2$) | $\leq$ 0.018 | $\leq$ 0.06 | | 18 | | | | |
| HCO$^+$ (1–0) | 0.04 | 0.052 | 0.75 | 18 | | | | |
| H$^{13}$CO$^+$ (1–0) | $\leq$ 0.03 | $\leq$ 0.11 | | 37 | | | | |
| DCO$^+$ (2–1) | $\leq$ 0.02 | $\leq$ 0.07 | | 23 | | | | |
| CCH | $\simeq$ 0.02 | $\simeq$ 0.09 | $\simeq$ 0.2 | 31 | | | | |

Upper limits are calculated at the 3$\sigma$ level with a line width of 0.3 km s$^{-1}$.
All data are given in $T_A^*$. The offset are given in arcsec, in equatorial coordinates relative to the source center.
[a] The C$^{18}$O(2–1) data are given as the average of three positions, (0,−180), (0,−190) and (0,−200) to improve the signal to noise ratio.

5 magnitudes, and a total column density of $H_2$ of 5 $10^{21}$ cm$^{-2}$ for the Polaris core.

Contrary to the high latitude core, the core in Taurus seems affected by selective photodissociation since the C$^{18}$O lines are much fainter compared to $^{13}$CO lines. The $^{13}$CO column density deduced from LVG is about the same as toward Polaris but the C$^{18}$O column density is 4 times lower: about 2 $10^{14}$ cm$^{-2}$ instead of 8 $10^{14}$ cm$^{-2}$. In this cloud, the abundance ratio [$^{13}$CO]/[C$^{18}$O] is significantly larger than the elemental abundance ratio, 34 versus 7, indicating that the UV radiation field has still an effect on the chemistry. Using also the star counts data from Duvert et al. (1986) to estimate the total extinction and the $H_2$ column density, we obtain $A_v$ = 3.5 mag from $^{13}$CO and $A_v$ = 2 mag from C$^{18}$O. Assuming an abundance for $^{13}$CO relative to $H_2$ of 2 $10^{-6}$, we obtain an $H_2$ column density of 3.1 $10^{21}$ cm$^{-2}$, consistent with the estimations of the extinction given above.

### 3.3.2. CS and C$^{34}$S

To derive abundances from the CS and C$^{34}$S data, we also used an LVG model with a kinetic temperature of 10 K and a solar isotopic ratio for sulfur [$^{32}$S]/[$^{34}$S] = 22.5, as there is no current evidence of large variation of this ratio in the interstellar medium (Wilson & Rood 1994; Kahane et al. 1988; Chin et al. 1996).

We have not included in this analysis the possible effect of electrons in the collisional excitation of CS because it is unlikely in dense cores: in order for electrons to compete with $H_2$ in the rotational excitation of CS, the electronic fractional abundance has to be larger than about $10^{-5}$ since the collision rates for CS with electrons are $2 \times 10^4$ larger than the collision rates for CS with $H_2$ (Drdla et al. 1989). Even in the HIP, such a high electronic abundance is not possible to achieve in well shielded clouds like Polaris and Taurus.

Apart from the position (37.5″,7.5″) in Polaris, the (2–1)/(3–2) temperature ratio towards most positions is between 2 and 3, both for CS and C$^{34}$S. In this regime and for a given J=2–1 line intensity, the CS column density varies roughly as the inverse of the $H_2$ density and can be written as:
$N(CS) = X(CS)\ n(H_2)\ L = 10^{14}\,\mathrm{cm}^{-2} \times (\Delta v/1\,\mathrm{km s}^{-1}) \times (10^4\,\mathrm{cm}^{-3}/n(H_2))$
where L is the size of the core along the line of sight. From a CS(3–2) map (Falgarone et al. 1996), we can estimate L to be of the order of 5 $10^{17}$ cm. Thus the CS relative abundance deduced from the LVG model is:
$X(CS) = 10^{18}/(n(H_2)^2 \times L) \simeq 2/n(H_2)^2$
with the $H_2$ density expressed in cm$^{-3}$. This restricts the range of possible densities to $n(H_2) \geq 10^4$ cm$^{-3}$.

On the other hand, a maximum value for the density is of about 2 $10^5$ cm$^{-3}$ for these positions since the CS(3–2) line is clearly weaker than the CS(2–1) line. The possible range of solutions for the CS column density is therefore huge, nearly a factor 20. In order to obtain conservative estimates of column densities, we give in Table 5 values of the CS and C$^{34}$S column densities for an $H_2$ density of $10^5$ cm$^{-3}$. This should therefore provide lower limits to the actual column density if the density were smaller than $10^5$ cm$^{-3}$.

The physical conditions along the line of sight towards position (37.″5,7.5″) in Polaris are different: the CS(2–1) and (3–2) lines have nearly the same strength while the J=2–1 line for C$^{34}$S and $^{13}$CS is twice stronger than the J=3–2 line. Similar

**Table 4.** Observed data towards Polaris

| Line | (1) (0″,0″) | | | | (2) (37.5″,7.5″) | | | | (3) (−7.5″,37.5″) | | | |
|---|---|---|---|---|---|---|---|---|---|---|---|---|
| | $\int T_A^* dv$ (K km s$^{-1}$) | $T_{max}$ (K) | $\Delta v$ (km s$^{-1}$) | $\sigma$ (mK) | $\int T_A^* dv$ (K km s$^{-1}$) | $T_{max}$ (K) | $\Delta v$ (km s$^{-1}$) | $\sigma$ (mK) | $\int T_A^* dv$ (K km s$^{-1}$) | $T_{max}$ (K) | $\Delta v$ (km s$^{-1}$) | $\sigma$ (mK) |
| $^{12}$CO(1–0) | 9.0 | 4.5 | 1.9 | 250 | 10.6 | 5.6 | 1.8 | 320 | 8.7 | 4.2 | 1.9 | 310 |
| $^{12}$CO(2–1)[a] | 4.0 | 2.5 | 1.6 | 218 | 6.3 | 2.3 | 1.6 | 190 | 5.5 | 3.0 | 1.6 | 210 |
| $^{13}$CO(1–0) | 3.6 | 5.2 | 0.65 | 200 | 3.4 | 5.3 | 0.60 | 410 | 2.7 | 4.8 | 0.53 | 370 |
| $^{13}$CO(2–1) | 2.2 | 3.2 | 0.65 | 120 | 1.7 | 3.4 | 0.46 | 380 | 2.0 | 3.7 | 0.51 | 150 |
| C$^{18}$O(1–0) | 1.1 | 1.9 | 0.52 | 210 | 0.77 | 2.0 | 0.37 | 150 | 0.71 | 1.7 | 0.38 | 160 |
| C$^{18}$O(2–1) | 0.58 | 1.1 | 0.49 | 96 | 0.64 | 1.5 | 0.39 | 120 | 0.47 | 1.1 | 0.41 | 75 |
| CS(2–1) | 0.85 | 1.5 | 0.52 | 76 | 1.0 | 2.3 | 0.43 | 130 | 0.47 | 1.0 | 0.45 | 80 |
| CS(3–2) | 0.48 | 0.79 | 0.56 | 78 | 0.99 | 2.0 | 0.47 | 130 | 0.30 | 0.49 | 0.58 | 87 |
| CS(5–4) | $\leq 0.27$ | $\leq 0.50$ | | 140 | $\leq 0.23$ | $\leq 0.50$ | | 150 | $\leq 0.23$ | $\leq 0.50$ | | 150 |
| C$^{34}$S(2–1) | 0.12 | 0.18 | 0.6 | 20 | 0.18 | 0.47 | 0.34 | 22 | 0.05 | 0.09 | 0.52 | 20 |
| C$^{34}$S(3–2) | $\leq 0.02$ | $\leq 0.04$ | | 13 | 0.05 | 0.17 | 0.27 | 32 | $\leq 0.05$ | $\leq 0.1$ | | 15 |
| $^{13}$CS(2–1) | | | | | 0.05 | 0.17 | 0.29 | 27 | | | | |
| $^{13}$CS(3–2) | | | | | 0.02 | 0.10 | 0.23 | 26 | | | | |
| SO($3_2$–$2_1$) | 0.30 | 0.57 | 0.50 | 67 | 0.33 | 0.72 | 0.43 | 90 | 0.17 | 0.39 | 0.42 | 55 |
| SO($4_3$–$3_2$) | 0.085 | 0.24 | 0.34 | 65 | 0.18 | 0.45 | 0.39 | 83 | 0.05 | 0.14 | 0.34 | 50 |
| $^{34}$SO($3_2$–$2_1$) | $\leq 0.02$ | $\leq 0.04$ | | 13 | $\leq 0.02$ | $\leq 0.04$ | | 13 | | | | |
| $^{34}$SO($4_3$–$3_2$) | $\leq 0.03$ | $\leq 0.06$ | | 21 | $\leq 0.03$ | $\leq 0.06$ | | 20 | | | | |
| HCO$^+$ (1–0) | 1.2 | 1.9 | 0.61 | 100 | 1.4 | 2.3 | 0.56 | 110 | 1.0 | 1.9 | 0.52 | 110 |
| H$^{13}$CO$^+$(1–0) | 0.2 | 0.47 | 0.40 | 55 | 0.39 | 0.75 | 0.49 | 58 | 0.17 | 0.38 | 0.41 | 63 |
| HC$^{18}$O$^+$ (1–0) | | | | | 0.06 | 0.06 | 1.0 | 20 | | | | |
| DCO$^+$(2–1) | 0.04 | 0.13 | 0.31 | 30 | 0.07 | 0.15 | 0.42 | 37 | | | | |
| CCH (3/2,2–1/2,1) | 0.28 | 0.74 | 0.36 | 25 | 0.64 | 1.5 | 0.40 | 30 | | | | |
| CCH (3/2,1–1/2,0) | 0.14 | 0.39 | 0.34 | 25 | 0.39 | 0.93 | 0.39 | 30 | | | | |
| $C_3H_2$($2_{12}$–$1_{01}$) | | | | | 0.39 | 1.1 | 0.34 | 34 | | | | |
| HCS$^+$(2–1) | | | | | 0.04 | 0.15 | 0.25 | 33 | | | | |

All data are given in $T_A^*$.
We have used the $^{12}$CO, $^{13}$CO and C$^{18}$O data of the IRAM KP.
The offset are given in arcsec, in galactic coordinates relative to the source center.
[a] Two lines for the gaussian fit

intensities for the (2–1) and (3–2) CS lines occur at very high densities only, n($H_2$) $\simeq 10^6$ cm$^{-3}$. However at such high densities, the C$^{34}$S lines should have the same intensity ratio as the CS lines. A possible explanation may therefore be the presence of lower density gas along the line of sight which absorbs and diffuses the CS(2–1) emission. In that case, the lower J lines are most affected and the observed intensity ratio is lower than the actual intensity ratio in the dense core gas. Because this effect is important for the main isotope only, we choose to use the information from the C$^{34}$S and $^{13}$CS data to determine the CS column density for this position. At an $H_2$ density of $10^5$ cm$^{-3}$, the C$^{34}$S and $^{13}$CS (2–1)and (3–2) data are well fitted with column densities N(C$^{34}$S) = 1.1 $10^{12}$ cm$^{-2}$ and N($^{13}$CS) = 3.7 $10^{11}$ cm$^{-2}$. Using the isotopic ratios [$^{32}$S]/[$^{34}$S] = 22.5 and [$^{12}$C]/[$^{13}$C] = 70, we obtain a CS column density of 2.5–2.6 $10^{13}$ cm$^{-2}$, with a remarkable agreement between the two isotopomers.

At a density of $10^5$ cm$^{-3}$, and with the observed line intensities, the excitation temperature for the CS and C$^{34}$S lines scatter around 5 K with larger values for the 2–1 line (6 to 7 K) than for the 3–2 line (4 to 5 K). Hence we give also in Table 5 the C$^{34}$S column densities assuming LTE at an excitation temperature of 5 K. Note that the change from 5 K to 4 K for $T_{ex}$ corresponds to an increase by a factor 1.5 in the column densities for CS; the change from 5 K to 8 K corresponds to a decrease of the column density by a factor 1.3.

The CS lines towards Taurus are much weaker than towards Polaris and we were unable to detect C$^{34}$S. While the CS/C$^{34}$S line ratio lies between 5 and 10 in Polaris, we obtain a 3$\sigma$ upper limit on the C$^{34}$S (2–1) line of 0.06 K, which can be converted to a 3$\sigma$ lower limit for the isotopic ratio of 5. The CS lines seem thus to be less saturated in this core than in Polaris. With an excitation temperature of 5 K, the expected brightness temperature of the C$^{34}$S (2–1) line is 14 mK, assuming the same line width as the CS line. This is well below our detection limit.

The much stronger CS and C$^{34}$S lines towards Polaris than towards Taurus result in much larger CS column densities towards the former core: in Polaris the CS column densities are a factor 10 to 40 higher than in Taurus although their $H_2$ column densities differ by less than a factor two.

**Table 5.** Column densitites

| | Polaris | | | Taurus | |
|---|---|---|---|---|---|
| Species | (0″,0″) | (37.5″,7.5″) | (−7.5″,37.5″) | (0″,−180″) | (0″,−190″) |
| $^{13}$CO | 6.8 $10^{15}$ | 6.2 $10^{15}$ | 4.2 $10^{15}$ | 6.2 $10^{15}$ | |
| C$^{18}$O | 9.3 $10^{14}$ | 7.5 $10^{14}$ | 6.5 $10^{14}$ | 1.8 $10^{14}$ | 1.6 $10^{14}$ |
| $H_2$ [a] | 5.7 $10^{21}$ | 5.2 $10^{21}$ | 3.5 $10^{21}$ | 3.5 $10^{21}$ | |
| C$^{34}$S [b] | 7.5 $10^{11}$ | 1.3 $10^{12}$ | 3.1 $10^{11}$ | $\leq$ 1.1 $10^{11}$ | $\leq$ 3.8 $10^{11}$ |
| C$^{34}$S [c] | 6.5 $10^{11}$ | 1.1 $10^{12}$ | 3.1 $10^{11}$ | | |
| $^{13}$CS [c] | | 3.7 $10^{11}$ | | | |
| CS [d] | 5–15 $10^{12}$ | 6–25 $10^{12}$ | 2.6–6.7 $10^{12}$ | 6.0 $10^{11}$ | 5.8 $10^{11}$ |
| SO [e] | 7.0 $10^{12}$ | 8.0 $10^{12}$ | 3.4 $10^{12}$ | 2.0 $10^{12}$ | 1.8 $10^{12}$ |
| $^{34}$SO [e] | $\leq$ 7.9 $10^{11}$ | $\leq$ 7.9 $10^{11}$ | | $\leq$ 3.6 $10^{11}$ | |
| H$^{13}$CO$^+$ | 2.7 $10^{11}$ | 5.8 $10^{11}$ | 2.3 $10^{11}$ | $\leq$ 3.7 $10^{10}$ | |
| DCO$^+$ | 6 $10^{10}$ | 1 $10^{11}$ | | $\leq$ 3.6 $10^{10}$ | |
| HCO$^+$ [f] | 1.9 $10^{13}$ | 4.1 $10^{13}$ | 1.6 $10^{13}$ | 5.0 $10^{10}$ | |
| HC$^{18}$O$^+$ [f] | | 7.4 $10^{10}$ | | | |
| HCS$^+$ [e] | | 3 $10^{11}$ | | | |
| CCH [g] | 1.5 $10^{13}$ | 3.4 $10^{13}$ | | $\simeq$ 1.1 $10^{12}$ | |
| $C_3H_2$ [h] | | 9. $10^{12}$ | | | |

All column densities are given in cm$^{-2}$.
[a] N($H_2$) is estimated from N($^{13}$CO) with [$^{13}$CO]/[$H_2$] = 1.2 $10^{-6}$ in Polaris and 2 $10^{-6}$ in Taurus (see text).
[b] N(C$^{34}$S) calculated from the (2–1) data with $T_{\rm ex}$ = 5 K
[c] N(C$^{34}$S) and N($^{13}$CS) are calculated with the LVG model with a density of 1. $10^5$ cm$^{-3}$
[d] N(CS) is calculated from N(C$^{34}$S) with [C$^{32}$S]/[C$^{34}$S] = 22.5 (high values) and/or from the CS data with the LVG model (low values)
[e] calculated in LTE with $T_{ex}$ = 5 K
[f] N(HCO$^+$) is calculated from N(H$^{13}$CO$^+$) with [HCO$^+$]/[H$^{13}$CO$^+$] = 70; N(H$^{13}$CO$^+$) is calculated in LTE with $T_{\rm ex}$ = 5 K.
[g] calculated in LTE with $T_{\rm ex}$ = 10 K
[h] see text

### 3.3.3. SO and $^{34}$SO

Because the dipole moment of SO is somewhat smaller than the dipole moment of CS on one hand, and the opacity of the individual lines are smaller for the same total column density on the other hand, we expect the excitation temperature of SO levels to be roughly the same as for CS levels of similar energy. We have therefore computed the SO column densities assuming LTE at a temperature of 5 K with a correction for finite optical depth, $\frac{\tau}{1-exp(-\tau)}$ valid for moderate optical depths. Indeed, we were unable to detect $^{34}$SO lines down to a temperature ratio, estimated with conservative $3\sigma$ upper limits, of SO/$^{34}$SO = 6 for Taurus and about 10 for Polaris, while the observed CS/$^{34}$CS temperature ratio are 8 and 5 for the two positions in Polaris. With such an excitation temperature, the opacity of the SO lines always stays below 1 for the observed positions, with a maximum of 0.5 for the position (37.5″,7.5″) in Polaris. The LTE SO column densities are therefore reliable within about a factor two in these clouds. There is a smaller difference between Polaris and Taurus SO column densities than between their CS column densities: the SO column densities towards Polaris are a factor four larger than towards Taurus.

### 3.3.4. HCO$^+$ and DCO$^+$

We have observed HCO$^+$ as one of the most abundant molecular ion in dark clouds. Towards Polaris, the line is strong and we were able to detect H$^{13}$CO$^+$, HC$^{18}$O$^+$, and DCO$^+$. Lines of isotopomers have moderate opacities and we calculate the column densities at LTE with an excitation temperature of 5 K, with the same correction for finite optical depth as given for the SO lines. We have checked with an LVG model, that the excitation temperature of H$^{13}$CO$^+$ is indeed close to 5 K at a density of $10^5$ cm$^{-3}$ and a kinetic temperature of 10 K. With a [$^{12}$C]/[$^{13}$C] abundance ratio of 70, the HCO$^+$ column density deduced from the H$^{13}$CO$^+$ data is 4 $10^{13}$ cm$^{-2}$ at the maximum position. Hence the HCO$^+$(1–0) line is saturated. A good fit of the observed brightness of the HCO$^+$ line, 2 K, is obtained with a density of 3 000 cm$^{-3}$ and a column density as given by H$^{13}$CO$^+$, N(HCO$^+$) = 4.1 $10^{13}$ cm$^{-2}$.

Using the same excitation temperature, 5 K, for the HC$^{18}$O$^+$(1–0) line, we derive a column density of HC$^{18}$O$^+$ of 7.4 $10^{10}$ cm$^{-2}$, which corresponds to an HCO$^+$ column density of 500 × 7.4 $10^{10}$ = 3.7 $10^{13}$ cm$^{-2}$, in very good agreement with the estimation from H$^{13}$CO$^+$.

The main surprise is the very low deuterium fractionation observed in this cloud: it is common to observe DCO$^+$ lines stronger than H$^{13}$CO$^+$ lines, revealing the high degree of deuterium fractionation in dark clouds: [DCO$^+$]/[HCO$^+$] = 0.05 on average (Guélin et al. 1982; Butner et al. 1995). Towards Polaris the DCO$^+$ lines are 5 times weaker than the H$^{13}$CO$^+$ line: assuming the same excitation temperature of 5 K, the DCO$^+$ column densities are 0.6 $10^{11}$ cm$^{-2}$ and 1 $10^{11}$ cm$^{-2}$ for the two observed positions, much smaller than the H$^{13}$CO$^+$ column densities at the same positions. This shows that the deu-

terium fractionation is very low in this cloud: $[DCO^+]/[HCO^+] = [DCO^+]/[H^{13}CO^+]/70 = 0.003$. Excitation effects are not likely to play a major role in the derivation of this ratio since it is established by comparing two optically thin lines. Moreover, densities derived from the excitation of $DCO^+$ generally agree with those derived from other molecules with large dipole moments such as CS and $C_3H_2$ (Butner et al. 1995). Because the CS and $C^{34}S$ data reveal the presence of dense gas, the excitation conditions of CS and $HCO^+$ and its isotopomers should be similar and the assumed value of 5 K for the excitation temperature of $DCO^+$ and $H^{13}CO^+$ fairly good.

Towards Taurus, the $HCO^+$ line is weak and broad. Assuming an excitation temperature between 4 and 5 K, the column density is about $5\ 10^{10} cm^{-2}$ and the line is optically thin.

### *3.4. Other species*

Because carbon is predicted to be more abundant in the HIP than in the LIP, a main consequence is the increased abundance of hydrocarbons in the HIP. We have thus observed the simplest carbon chain CCH towards both cores and have indeed detected strong lines towards Polaris (Fig 1 and 2, Tables 3 and 4). The CCH lines in Polaris are among the strongest lines detected in dark clouds: Wootten et al. (1980) established the presence of CCH in molecular clouds and found lines up to 2 K in dark cores. However, this survey was done with a large beam (3'), and a detailed comparison of Polaris with other dark clouds will await higher resolution and better signal to noise data. In Polaris, the CCH peak antenna temperature is 1.5 K and the CCH column density derived for $T_{ex} = 10$ K is $3\ 10^{13}\ cm^{-2}$. The corresponding CCH relative abundance to $H_2$ is about $8\ 10^{-9}$. CCH is barely detected towards Taurus with a peak antenna temperature of about 0.09 K, fifteen times fainter than towards Polaris.

We have also detected the cyclic hydrocarbon $C_3H_2$ toward one position in the same cloud. The excitation of $C_3H_2$ is fairly complex and it is thus difficult to deduce a column density from one line only. Using the LVG calculations of Cox et al. (1989), and assuming that the excitation conditions of $C_3H_2$ are the same in Polaris as in other dense cores, we deduce a column density of $9\ 10^{12}\ cm^{-2}$. Thus the $C_3H_2$ abundance is $2\ 10^{-9}$ in Polaris, a value well in the range of abundances found in dark clouds, 0.3–4 $10^{-9}$ (Cox et al. 1989).

Finally, we have detected the molecular ion $HCS^+$, with a column density of $3\ 10^{11}\ cm^{-2}$ assuming the same excitation temperature as $C^{34}S$ and SO: $T_{ex} = 5$ K. Thus the $[HCS^+]/[CS]$ abundance ratio is about 0.012, a value similar to those found in dark clouds, 0.01 to 0.07 (Thaddeus et al. 1981; Hirahara et al. 1992). This lends support to the high CS column densities derived from the analysis of the $C^{34}S$ and $^{13}CS$ data.

### *3.5. Uncertainties and artefacts*

We would like to stress that the determination of densities and column densities in this paper, as well as most of the determinations in the litterature, suffer from severe uncertainties. We can put the possible sources of errors into different categories:

– First of all, the uncertainty on the measurement itself. The line calibration is not accurate to better than about 20%. Then, depending on the temperature scale used, $T_A^*$ versus $T_{mb}$, the uncertainty on the absolute brightness temperature of the highest frequency observed line amounts to 30 to 100 % and affects the line ratios by large factors. Finally, because large antennas have important error patterns at high frequencies which vary with the exact observing frequency, the observed line strength may be contaminated by emission in the side lobes. This effect should not be too serious in our case, since we observed towards local maxima but is more important for cloud edges.

– The most important effect is due to the assumptions in the LVG models. First, independently of the actual density structure of the dense cores, the LVG formalism can only provide estimates of the density and column density from a given observed set of nearby rotational transitions, and the uncertainty is about an order of magnitude. In addition, the actual structure of a dense core is far from the uniform density assumed by the LVG models. Models with density gradients might be more appropriate to describe the observed signals. But such models require more complete data sets to be used because they have a larger number of free parameters to fit.

– The presence of high density cores has also a consequence for the radiative transfer of the line emission: molecules in the lower density gas are expected to be radiatively excited by the emission of the high density cores and to scatter the emission of the cores. This effect is most important for high dipole moment molecules. It has been studied in TMC1 for $HCO^+$ by Cernicharo & Guélin (1987) for example. The width of the $HCO^+$ lines, similar to that of $^{13}CO$, is indeed an evidence of radiatively excited emission of low density gas.

– Finally the values of isotopic ratio are uncertain too. Since isotopomers are observed because their lines are less saturated, the final column density depends on the the assumed isotopic ratio. The status of isotopic ratio in the interstellar medium is discussed by Wilson & Rood (1994).

In conclusion, the determinations of the absolute values of molecular column densities suffer from large uncertainties, but the comparison of these column densities among two cores which have comparable $^{13}CO$ column density, velocity dispersion and density (and therefore comparable excitation temperature for the observed lines) is most likely meaningful and it is what is discussed in the following section.

## 4. Abundances and comparison with other dark clouds

### *4.1. CS and SO*

We have plotted on Figures 3a and 3b the abundances of CS and SO relative to $C^{18}O$: $N(CS)/N(C^{18}O)$ and $N(SO)/N(C^{18}O)$ as a function of $N(C^{18}O)$. We also show the abundance ratio $N(CS)/N(SO)$ as a function of the $C^{18}O$ column density in Figure 3c. We chose to compare all the molecular column densities to that of $C^{18}O$ rather than that of $^{13}CO$ because the former is a

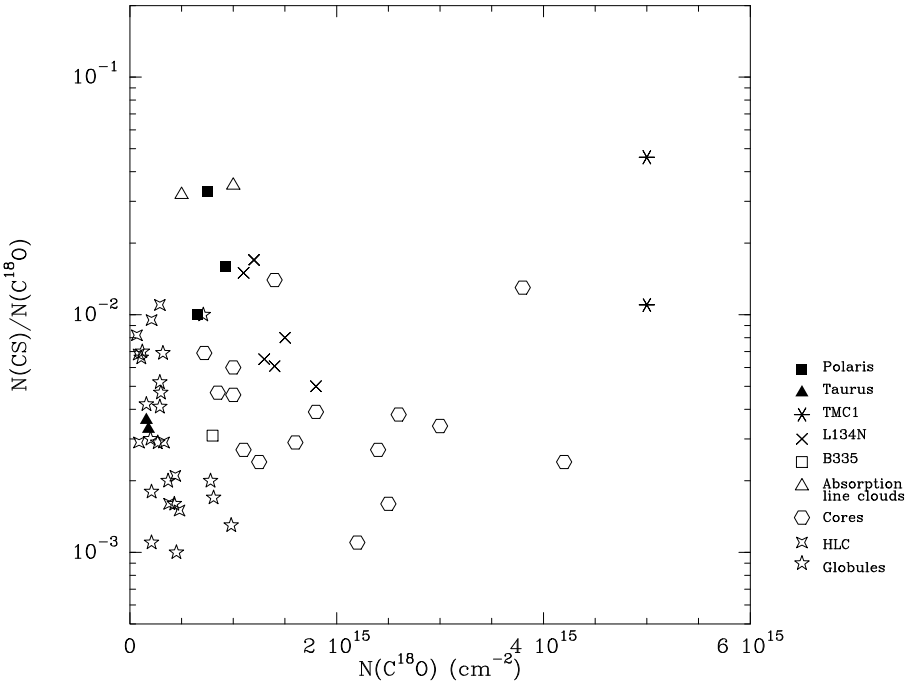


**Fig. 3a.** Column density ratio N(CS)/N($C^{18}O$) as a function of the $C^{18}O$ column density for Polaris (black squares), Taurus (black triangles), TMC1 (asterisks), L134N (crosses), B335 (white square), clouds seen in absorption (white triangles), dark clouds cores (white hexagons), high latitude clouds (starred squares) and globules (stars)

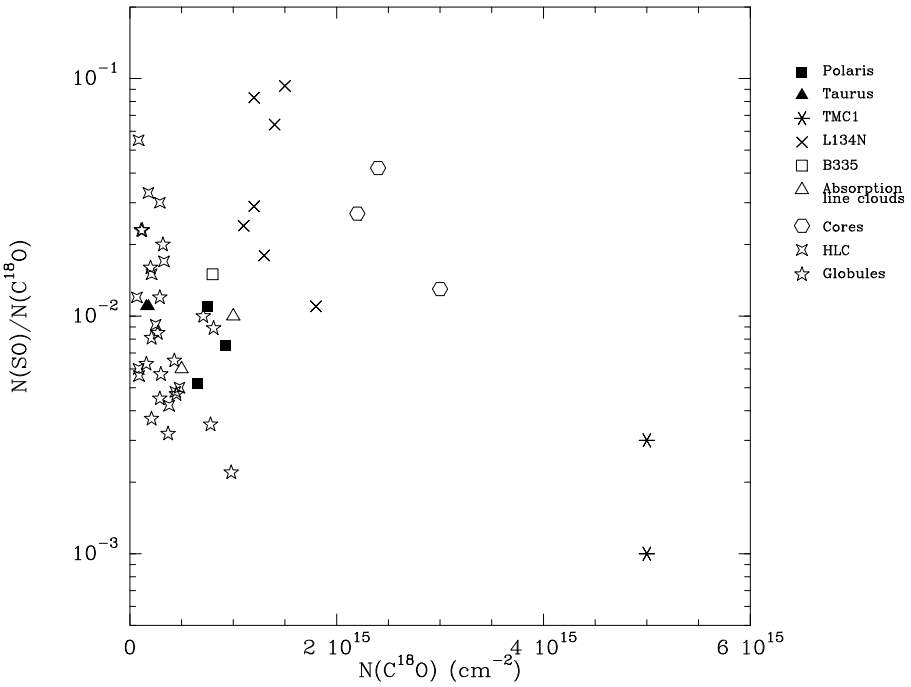


**Fig. 3b.** Same as for Fig. 3a for the column density ratio N(SO)/N($C^{18}O$)

better tracer of the opaque parts of the cores where chemical bistability is most likely to occur.

The solid squares represent the points for Polaris and the solid triangles those for Taurus. We have added a few observations of the L134N dark cloud (Swade 1989a,b) as crosses and of TMC1 (Hirahara et al. 1992 for CS; Hirahara et al. 1995 for SO and Schilke et al. 1995 for $C^{18}O$) as asterisks. As a representative dark cloud, we have also used the core abundances of B335, outside the collapse region (Frerking et al. 1987; M. Gerin private communication) (squares). The open triangles correspond to absorption line data quoted in Tieftrunk et al. (1994) . Data for other dark cloud cores have been collected in the literature, using the SO survey by Rydbeck et al. (1980) & the CS survey by Zhou et al. (1989). These points are drawn as open hexagons. Finally, we have used the survey data from Turner (1996 for CS, 1995b for SO; 1993, 1994 and Turner at al. 1992 for $C^{18}O$) on high latitude cloud cores and dark globules of Clemens & Barvainis (1988). These points are drawn as starred squares and stars.

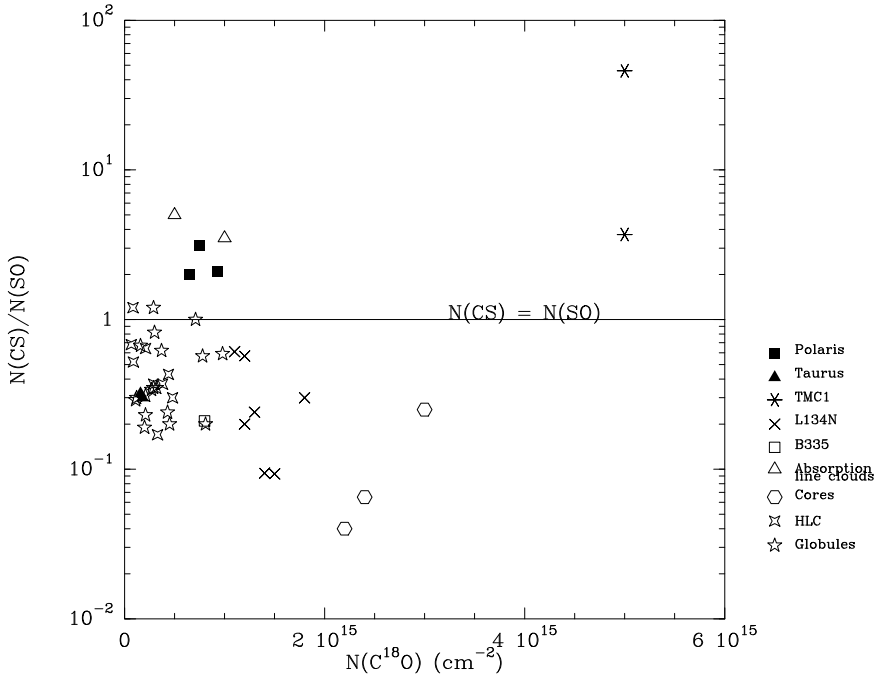


**Fig. 3c.** Same as for Fig. 3a and 3b for the column density ratio N(CS)/N(SO)

The dark clouds added for comparison have a total extinction comparable to or slightly larger than that of Polaris or Taurus. On the other hand, the objects in Turner's survey have mostly lower $C^{18}O$ column densities than Polaris. In order to treat all the data in a consistent way, we have recomputed, when possible, the CS and SO column densities from the published spectra. On this figure the points towards Polaris and towards the cyanopolyyne core in TMC1 stand out as having a rather large CS column density. In L134N the scatter of the SO abundances is large, but no point reaches comparable high CS and low SO column densities as towards Polaris.

CS and SO were chosen because their abundances are sensitive to the amount of available atomic carbon in opposite ways. As already mentioned, the production of CS is favoured by the presence of atomic carbon whereas SO is efficiently destroyed by this same species, in the reaction C + SO $\longrightarrow$ CO+ S. The formation of SO is mainly governed by the neutral-neutral reaction: S + OH $\longrightarrow$ SO + H.

Significant variations of the CS and SO abundances (Fig 3a and 3b) and of the [CS]/[SO] abundance ratio (Fig 3c) are observed: the [CS]/[SO] abundance ratio ranges from 0.1 to 40 in dark clouds and from 0.1 to 0.6 in a single dark cloud core L134N. Both the variations inside a given cloud (L134N) and from cloud to cloud point towards a particular chemical phenomenon which could be responsible for the huge range of observed values. A possible interpretation would involve the coexistence of regions with different chemical properties as those found in the bistability phenomenon which is discussed below.

### *4.2. Deuterium fractionation*

Apart from the strong CS and CCH lines, another unusual characteristic of the Polaris observations is shown in Fig. 4 which displays the deuterium fractionation ratio obtained from $H^{13}CO^+$ and $DCO^+$ data against the $C^{18}O$ column density in various clouds. We use data towards TMC1 and L134N from Guélin et al. (1982) and the survey of dense cores by Butner et al. (1995). The two points in Polaris stand out as having a very low fractionation ratio, a factor ten lower than the average fractionation ratio in dense cores, $[DCO^+]/[HCO^+] = 0.05$, found by Butner et al. (1995).

Indeed, deuterium fractionation is thought to occur mainly via the deuterium exchange reaction:

$H_3^+ + HD \longrightarrow H_2D^+ + H_2$

with subsequent transfer of the deuterium nucleus to more complex molecules in protonation reactions (Watson 1974). The main route to $DCO^+$ is thus:

$H_2D^+ + CO \longrightarrow DCO^+ + H_2$,

while for neutral species such as CCH, deuteration proceeds in two steps: a first step to produce a deuterated molecular ion followed by the dissociative recombination of this deuterated molecular ion to produce the deuterated neutral species. This is an efficient process in dark clouds since the deuterium fractionation reaches a few percents compared to the cosmic deuterium abundance $[D]/[H] \simeq 2\ 10^{-5}$ (Wootten 1987).

### *4.3. Comparison with models*

In order to interpret the observations we have built a chemical network which includes, in addition to H, He, C, N, O and S, the D and $^{13}C$ isotopes. The chemical network is an update of those published in Le Bourlot et al. (1993a), Pineau des Forêts et al. (1989), Pineau des Forêts et al. (1993) where photoreactions are included. We consider the deuteration of carbon, oxygen and nitrogen-containing species only. We have run a variety of models by sampling the range of the different control parame-

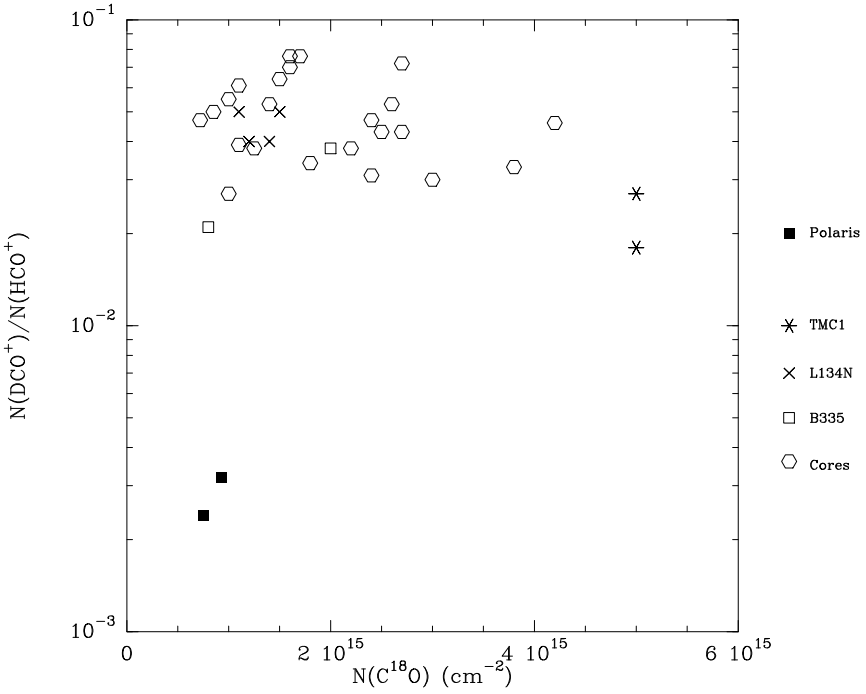


**Fig. 4.** Deuterium fractionation ratio $N(DCO^+)/N(HCO^+)$ as a function of the $C^{18}O$ column density. The symbols have the same meaning as in Fig. 3

ters such as density, temperature, cosmic ionization rate, visual extinction, C/O abundance ratio.... As shown in Le Bourlot et al. (1995a, b), all models exhibit bistability for values of the control parameters relevant to the interstellar medium. We do not try to find a specific agreement between observations and model calculations, but we rather want to derive general trends which may help to understand the observed abundance variations.

In Figure 5, we present an illustration of the fractional abundance variations, for a range of hydrogen densities $n_H = n(H) + 2n(H_2)$, predicted by our chemical models together with the observed values which are displayed at $n_H = 10^4\ cm^{-3}$ for convenience. Note that the model abundances are defined as density ratios $n(X)/n_H$ whereas the observed abundances are column densities ratios $N(X)/N_H = 2N(X)/N(H_2)$. Therefore, in such comparisons, we make the implicit hypothesis of an homogeneous medium with constant molecular abundances along the line of sight. Following the observations, we have taken a conservative value of the extinction $A_v$ equal to 5, a cosmic rays ionization rate of $5\ 10^{-17}\ s^{-1}$ and a temperature of 15K. We assume an incident radiation field of one half of the standard galactic ultra violet interstellar radiation and the standard galactic extinction law. The elemental abundances are those found in the $\zeta$ Oph environment as determined by Sofia, Cardelli & Savage (1994). They are listed in Table 6. Sulfur is taken to be depleted by a factor of 10. Each point in Fig. 5 corresponds to one specific solution of the steady state equations of the molecular abundances. For clarity we display the sole stable solutions, but we stress out that there is a branch of unstable solutions joining the two critical points at the ends of the two stable branches.

In the range of displayed densities, the ionization fraction of the HIP is about several times $10^{-6}$ whereas the value obtained in the LIP is of the order of $10^{-7}$. Figures 5 unambiguously

**Table 6.** Elemental abundances relative to H

| Element | Abundance |
|---|---|
| D | $2.0\ 10^{-5}$ |
| He | $1.0\ 10^{-1}$ |
| $^{12}C$ | $1.32\ 10^{-4}$ |
| $^{13}C$ | $1.47\ 10^{-6}$ |
| N | $2.47\ 10^{-5}$ |
| O | $2.92\ 10^{-4}$ |
| Si | $3.6\ 10^{-8}$ |
| S | $1.85\ 10^{-6}$ |
| Metals | $1.5\ 10^{-8}$ |

shows that large fractional abundances of CS, $C_2H$ and $HCS^+$ are only obtained in a High Ionization Phase. On the opposite, SO, $HCO^+$ and $DCO^+$ are characteristic species of the Low Ionization Phase. The simultaneous observation of several of the above molecular species in a given line of sight may then be an illustration of the occcurence of the two chemical phases in the dark cloud core. At $\zeta = 5\ 10^{-17}\ s^{-1}$, the range of densities where the two solutions may coexist is $2\,000\ cm^{-3}$ to $2\ 10^4\ cm^{-3}$, which encompasses the range derived from the $^{13}CO$ and $C^{18}O$ data. The upper and lower density boundaries are proportional to $\zeta$ as shown in Le Bourlot et al. (1995a).

As discussed above, deuteration mainly occurs via the transfer of deuteron in reactions of the key $H_2D^+$ molecular ion with neutral molecules such as CO and HCN. But reactions involving the atomic $D^+$ ion also play a role. The dissociative recombination cross sections of $H_2D^+$ are very close to those of $H_3^+$ (Datz et al. 1995). So, dissociative recombination may become competitive with fractionation reactions in the HIP, which reduces the production of deuterated molecules and molecular ions in

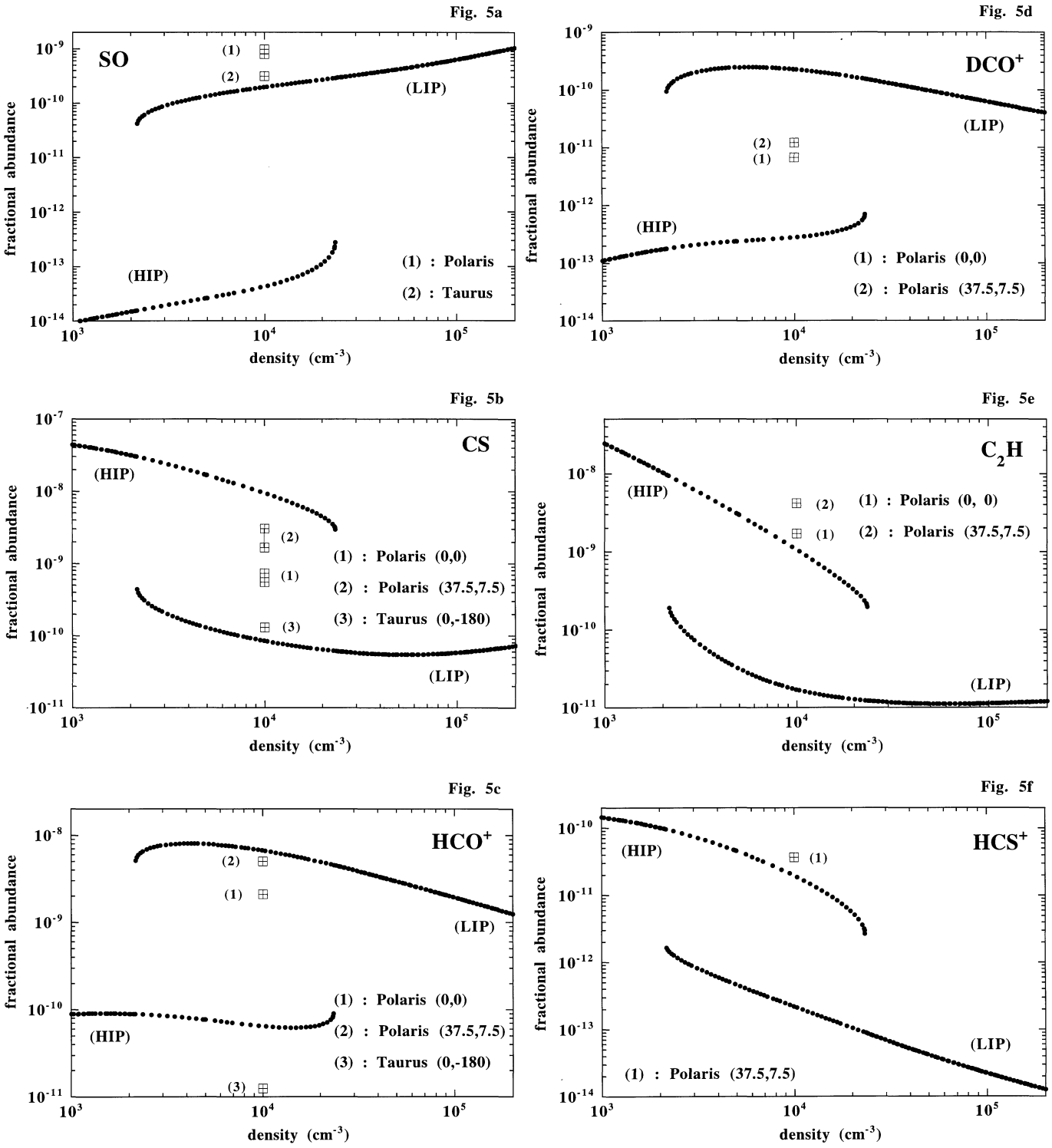


**Fig. 5a–f.** Fractional abundance of **a** SO, **b** CS, **c** $HCO^+$, **d** $DCO^+$, **e** CCH and **f** $HCS^+$ as a function of the gas density $n_H$ for the conditions given in the text. The HIP is the dominant phase at low densities while the LIP is dominant at high densities. The squares show the location of observed data. The abundances are given as density ratios, $n(X)/n_H$ where $n_H$ the total number of protons. Abundances relative to $H_2$ are therefore twice larger

this phase, leading to a decrease in the deuterium fractionation ratios.

In addition to an evidence for the presence of both stable phases in each field, the CS, $HCS^+$ and CCH diagrams suggest that the fraction of HIP in the Polaris field is, as expected, larger than in the Taurus field. The fact that the measured fractional abundance of $DCO^+$ lies in between the two LIP and HIP solutions may be an illustration of the mixing of the two phases along the line of sight. However, two species apparently weaken this conclusion: SO and $HCO^+$. The SO abundance is highly sensitive to gas temperature in the 5K to 20K interval due to the small energy barrier assumed in the neutral-neutral reaction $S + OH \longrightarrow SO + H$ which is the main formation route of SO. As for $HCO^+$, it is quite possible that the observed lines are not specific of the dark cores but carry an important contribution from the low density envelope. The broad $HCO^+$ line widths, comparable to that of the $^{13}CO$ lines suggest that scattering by the envelope gas may alter the core signal, even for the $H^{13}CO^+$ line which we used to measure the $HCO^+$ column density. In that case, the measured signal reflects the $HCO^+$ abundance both in the dark core and in the external envelope. Yet other processes involving chemical patterns specific to regions heated by the dissipation of turbulence might be involved (Falgarone et al. 1995). Further observations are needed to elucidate this point.

## 5. Discussion: How to interpret abundance variations and the relation with chemical bistability?

The possibility to test any astrophysical model relies on the ability to derive meaningful physical observables from the observations on the one hand, and to compute similar observables with a model on the other hand. For interstellar chemistry, the observed signal toward a particular position in a dark cloud reflects a complex average of the actual physical conditions along the line of sight. The column densities and relative abundances determined through the observations of a set of rotational lines of a given molecule are therefore averages both in the beam and along the line of sight. On the contrary, chemical models predict local abundances for a piece of gas with well defined parameters. Any confrontation of chemical models with observations must therefore recognize the fact that lots of effects are not taken into account by the models. For gas phase chemistry, the most noticeable effect is the spatial structure of the interstellar medium, which would require to run hydrodynamical simulations coupled with chemical models. De Boisanger et al. (1991, 1992) have shown that moderate variations of a cloud illumination resulted in enhanced gas cooling and the transient formation of dense clumps in diffuse clouds (initial density $n_H \simeq 50\,cm^{-3}$) with a large contrast with the surrounding medium. Turner (1993, 1994, 1995a & 1995b, 1996) has surveyed high latitude clouds and globules in $C^{18}O$ and a number of other molecular lines. He interprets the data with an assumed physical structure for the cloud and simple chemical models. The physical structures proposed are either polytropes, power law densities or self-similar collapse. Among the studied species, the sulfur monoxyde exhibits the largest abundance variations from

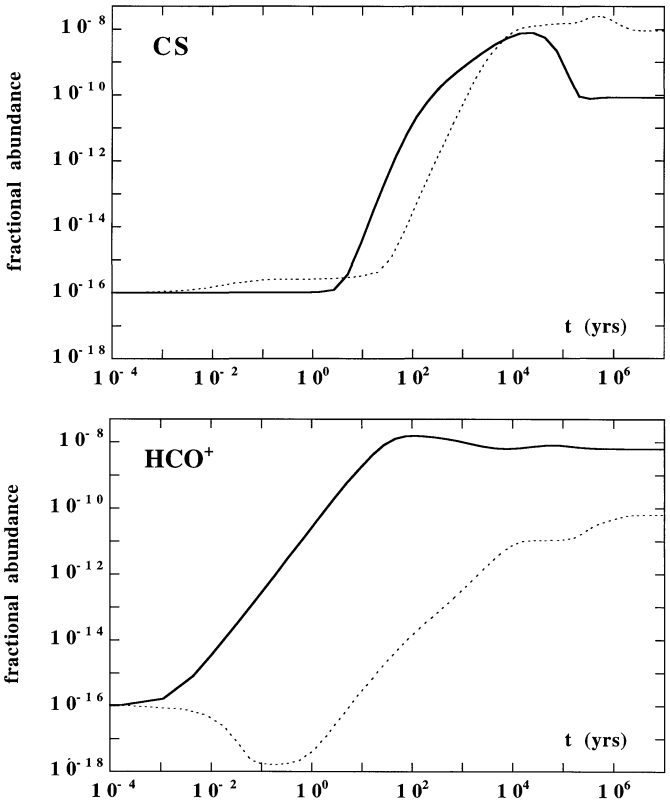


**Fig. 6a and b.** Fractional abundance of CS and $HCO^+$ as a function of time for two initial conditions. In both cases, $n_H = 10^4\,cm^{-3}$ and $\zeta = 5\,10^{-17}\,s^{-1}$; the full line represents the evolution of a molecular cloud composed of $H_2$, CO, O and $O_2$, $H_2S$ and N at t=0., while the dashed line represents the evolution of an atomic cloud composed of H, $C^+$, O, $S^+$ and N at t=0. The former model naturally converges towards the LIP solution while the latter reaches the HIP solution

cloud to cloud. The outcome of this unique survey can be summarized as follows: – ion-molecule chemistry may explain the dominant trends in the observations of these clouds, – it proves to be very difficult to determine the physical structure from a few data points for each cloud, since the same measurements can be fitted almost equally well with different physical models and reasonable chemical abundances. For denser gas, even though attempts have been made to take into account important mechanisms linked to gas dynamics such as mixing (Chièze et al. 1991), turbulent diffusion (Xie et al. 1995), turbulent heating (Falgarone et al. 1995), much work remains to be done.

Even at the level of the chemical models themselves, improvements are needed: pure gas-phase chemistry is clearly unrealistic. Models involving a coupling between the gas phase and the solid phase (dust grains) also present the phenomenon of bistability (Le Bourlot et al. 1995b). Furthermore, time dependent effects in the chemistry may be relevant since the dynamical time scales of dense clouds is about $10^5$ years. To investigate how the initial conditions affect the evolution of dense gas and how fast the steady-state equilibrium is reached, we have followed the evolution towards steady state of two clouds with the same fixed density, $10^4\,cm^{-3}$, and ionization rate $\zeta =$

$5\ 10^{-17}\,s^{-1}$, but with different initial compositions: for both models, the gas is completely molecular at t=0 but carbon and oxygen are locked into different species. In Fig. 6 we show the evolution of the CS (top) and $HCO^+$ (bottom) relative abundances as a function of time for these two initial conditions. The full line describes the evolution of a completely molecular cloud, composed of $H_2$, CO, O and $O_2$, $H_2S$ and N at $t = 0$, while the dashed line corresponds to an atomic cloud composed of H, $C^+$, O, $S^+$ and N at the start of the calculation. As foreseen, the former case converges towards the LIP solution, while the latter reaches the HIP solution. The time to reach the steady state is different for CS, about $10^5$ years, and $HCO^+$, about 100 years. Note that CS and $HCO^+$ have been chosen as having rather extreme convergence time scales. For other species, intermediate values are found.

Due to the effects discussed above, we now need chemical models with spatial information to describe the observations, and cannot rely on the oversimplified semi-infinite slab models. Indeed, for bistability, the main question which arises is the smallest scale of the chemical heterogeneity, i.e. the scale at which a gas cell can be considered to have a homogeneous composition. For a piece of molecular gas with physical conditions (density and ionization rate) in the bistability range, a mixture of both phases is expected to occur, with neighbouring gas cells evolving between one phase or the other. Because the time to reach steady state abundances is different for different molecular species, and most importantly of the same order of magnitude as the dynamical timescale of cloud evolution, the difference between phases might even not be as clearcut as in steady state models and cycles or even chemical chaos might occur (Le Bourlot et al. 1995a). This theory therefore predicts the presence of chemical heterogeneities even at small scale in a given cloud, where the physical parameters are uniform. The marked difference of line shapes for different species observed toward TMC1 by Langer et al. (1995) might be a manifestation of such a "chemical chaos". It should be still possible to find line of sights dominated by one phase or the other, depending on the range of densities along the line of sight and ionization rate.

What would be the strategy to ascertain this phenomenon? Fortunately, not all the molecules have abundances as sensitive to control parameters as for instance CS. The choice of the species is therefore most important to be able to recognize the patterns predicted by chemical bistability. Because the bistability phenomenon is linked to the dissociative recombination of $H_3^+$ (Roueff et al. 1996), the emphasis has to be put on chemical processes involving this molecular ion such as protonation reactions. $N_2H^+$ is a direct product of protonation reactions and its abundance is thus expected to be very sensitive to the chemical phase. Deuterium fractionation reactions can be considered as a subclass of such reactions, with the advantage of involving isotopomers and thus of an easier confrontation of observations with model predictions. To obtain a more secure test, the existence of dark clouds with low fractionation has to be tested by further observations of other deuterated species.

A complementary approach is to observe also the species whose abundances are expected to present little variations between the phases. We find that HCN and HNC belong to this class with a ratio of fractional abundances which does not exceed 5 when the density is varied.

A thorough search for $N_2H^+$, CS, SO, CCH, CCD, $DCO^+$ and $H^{13}CO^+$, HNC, $HN^{13}C$ and DNC, in the dense cores which present the highest $C^{18}O$ column density would therefore be worthwhile.

Another test would be to establish the presence of a high abundance of neutral carbon in dense cores. However, since the cores are always surrounded by a more diffuse envelope, the carbon emission of the envelope dominates the emergent signal, and the line is optically thick (e.g. the case of TMC1, Schilke et al. 1995)

In conclusion, the present study unambiguously shows marked chemical differences in nearby similar clouds which cannot be interpreted in the framework of a standard steady state chemical model. The bistability phenomenon may provide a natural explanation for these inhomogeneities but testing the existence of chemical chaos in dark clouds clearly deserves further observational investigations.

*Acknowledgements.* We thank the IRAM staff for the help during the observations. This work has been done during a stay of M. Gerin at Caltech supported by a NATO grant. She thanks the director of the CSO, T. Phillips, for his hospitality. We also thank the CNRS–GdR "Physico-Chimie des Molécules et des Grains Interstellaires (PCMGI)" for financial support.

## References

Butner H.M., Lada E.A., Loren R.B., 1995, ApJ 448, 207
Cernicharo J., Guélin M., 1987, A&A 176, 299
Chièze J.P., Pineau des Forêts G., Herbst E., 1991, ApJ 373, 110
Chin Y.N., Henkel C., Whiteoak J.B., Langer N., Churchwell E.B., 1996, A&A 305, 960
Clemens D.P., Barvainis R., 1988, ApJS 68, 257
Cox P., Walmsley C.M., Güsten R., 1989, A&A 209, 382
Datz S., Sundstrom G., Biedermann C., Brostrom L., Danared H. Mannervik S., Mowat J.R., Larsson M., 1995, Phys. Rev. Letters 74, 896
Datz S., Larsson M., Stromholm C., Sundstrom G., Zengin V., Danared H., Kallberg A., Afugglas M., 1995, Phys. Rev. A 52, 2901
De Boisanger C., Chièze J.P., 1991, A&A 241, 581
De Boisanger C., Chièze J.P., Meltz B. 1992, ApJ 401, 182
Drdla K., Knapp G.R., Van Dishoeck E.F., 1989, ApJ 345, 815
Duvert G., Cernicharo J.,Baudry A., 1986, A&A 164, 349
Falgarone E., Pineau des Forêts G., Roueff E., 1995, A&A 300, 870
Falgarone E., Panis J.F., Heithausen A., Pérault M., Stutzki J., Puget J.L., Güsten R., Gerin M., 1996 (in preparation)
Flower D.R., Le Bourlot J., Pineau des Forêts G., Roueff E., 1994, A&A 282, 225
Frerking M.A., Langer W.D., Wilson T.L., 1982, ApJ 262, 590
Frerking M.A., Langer W.D., Wilson R.W., 1987, ApJ 313, 320
Grossmann V., Heithausen A., 1992, A&A 264, 195
Guélin M., Langer W.D., Wilson R.W., 1982, A&A 107, 107
Heiles C., 1976, ApJ 208, L137
Heithausen A., Corneliussen U., Grossmann V., 1995, A&A 301, 941
Herbst E., Leung C.M., 1989, ApJ suppl. 69, 271

Hirahara Y., Susuki H., Yamamoto S., 1992, ApJ 394, 539
Hirahara Y., Masada A., Kawaguchi K., Ohishi M., Ishikawa S., Yamamoto S., Takano S., Kaifu N., 1995, PASJ 47, 845
Kahane C., Gomez-Gonzalez J., Cernicharo J., Guélin M., 1988, A&A 190, 167
Keene J., 1995, in: *The Physics and Chemistry of interstellar Molecular Clouds*, pp 186–194, Winnewisser, G. Pelz, G.C. (eds.) Springer, Heidelberg
Lada C.J., Lada E.A., Clemens D.P., Bally J., 1994, ApJ 429, 694
Langer W.D., Graedel T.E., 1989, ApJ suppl. 69, 241
Langer W.D., Velusamy T., Kuiper T.B.H., Levin S., Olsen E., Migenes V., 1995, ApJ 451, 293
Le Bourlot J., Pineau des Forêts G., Roueff E., Flower D. R. 1993a, A&A 267, 233
Le Bourlot J., Pineau des Forêts G., Roueff E., Schilke P., 1993b, ApJ 416 Letter 87
Le Bourlot J., Pineau des Forêts G., Roueff E., 1995a, A&A 297, 251
Le Bourlot J., Pineau des Forêts G., Roueff E., Flower D., 1995b, A&A 302, 870
Millar T.J., Leung C.M., Herbst E., 1987, A&A 183, 109
Olano C.A., Walmsley C.M., Wilson T.L., 1988, A&A 196, 194
Phillips T.G., Huggins P.J., 1981, ApJ 251, 533
Pineau des Forêts G., Roueff E., Flower D.R., 1989, MNRAS 240, 167
Pineau des Forêts G., Roueff E., Flower D.R., 1992, MNRAS 258, 45P
Pineau des Forêts G., Roueff E., Schilke P., Flower D.R., 1993, MNRAS 262, 915
Roueff E., Pineau des Forêts G. and Le Bourlot J., 1996, in "Dissociative Recombination. Theory, experiments and applications" Zajfman, D.(ed.)(in press)
Rydbeck O.E.H., Irvine W.M., Hjalmarson A., Rydbeck G., Ellder J., Kollberg E., 1980, ApJ 235, L171
Schilke P., Keene J., Le Bourlot J., Pineau des Forêts G., Roueff E., 1995, A&A 294, L17
Sofia U. J., Cardelli J. A., Savage B. D., 1994, ApJ 430, 650
Swade D.A., 1989a, ApJ 345, 828
Swade D.A., 1989b, ApJ suppl. 71, 219
Thaddeus P., Guélin M., Linke R.A., 1981, ApJ 246, L41
Tieftrunk A., Pineau des Forêts G., Schilke P., Walmsley C.M., 1994, A&A 289, 579
Turner B.E., 1993, ApJ 405, 229
Turner B.E., 1995, ApJ 449, 635
Turner B.E., 1994, ApJ 420, 661
Turner B.E., 1995a, ApJ 449, 635
Turner B.E., 1995b, ApJ 455, 556
Turner B.E., 1996, ApJ 461, 246
Turner B.E., Xu L., Rickard L.J. 1992, ApJ 391, 158
Ungerechts H., Bergin E.A., Goldsmith P.F., Irvine W.M. Schloerb F.P. and Snell R.L., 1995, in *The Physics and Chemistry of interstellar Molecular Clouds*, pp 258– 264, Winnewisser, G., Pelz, G.C. (eds.) Springer, Heidelberg
Watson W.D., 1974, ApJ 188, 35
Wilson T.L., Rood R.T., 1994, ARAA 32, 191
Wootten A., 1987, IAU Symposium 120 "Astrochemistry", M.S. Vardya & S.P. Tarafdar eds, 311
Wootten A.H., Bozyan E.P., Garett D.B., Loren R.B., Snell R.L., 1980, ApJ 239, 844
Xie T., Allen M., Langer W.D., 1995, ApJ 440, 674
Zhou S., Wu Y., Evans N.J., Fuller G.A., Myers P.C., 1989, ApJ 346, 168